

Comparison of second-order Raman scattering measurements with a phonon density-of-states calculation in GaSb

P. B. Klein

Naval Research Laboratory, Washington, D. C. 20375

R. K. Chang*

Department of Engineering and Applied Science, Yale University, New Haven, Connecticut 06520

(Received 10 May 1976)

Second-order Raman measurements have been made on oriented GaSb with various combinations of incident and scattered polarizations in order to obtain the three irreducible components of the Raman tensor (Γ_1 , Γ_{15} , and Γ_{12}). The dominant Γ_1 Raman spectrum is compared with the recently reported one-phonon density of states calculation based upon shell-model parameters that were fitted to neutron data. Significant deviations exist and we believe these to be artifacts of the shell-model parameters used. The observed dependence of the $2LO(\Gamma)$ and $2TO(\Delta)$ Raman peaks upon incident photon energy was attributed to resonance Raman effect with the $E_1 + \Delta_1$ direct gap and with the $\Gamma_{15\nu} \rightarrow \Delta_{1c}$ indirect gap, respectively.

Good correlation between the second-order Raman spectrum and the density of one-phonon states [$g(\nu)$] (with its frequency scale expanded by 2) has been reported for Si,^{1,2} Ge,³ diamond,⁴ GaP,⁵ InSb,⁶ ZnTe,⁷ and GaSe.⁸ In fact, the shapes of the 2TA Raman spectra of all diamond and zinc-blende-type semiconductors measured thus far are similar to each other and to the characteristic shape of the $g(\nu)$. It is a well-established experimental fact that the second-order Raman spectra are characterized by a dominant Γ_1 component comprised mostly of overtones, a weaker Γ_{15} component due mainly to combinations, and a very weak Γ_{12} component. The $g(\nu)$ is usually calculated using the shell-model (SM) parameters, which are obtained by fitting to coherent inelastic-neutron-scattering data.^{9,10}

Recently Farr *et al.*¹¹ have calculated the $g(\nu)$ for GaSb (T_d^2 structure) by using the method of Gilat and Raubenheimer.¹² The SM parameters used were those that fitted their neutron data, which were confined to the three principal symmetry axes, $\langle 100 \rangle$, $\langle 111 \rangle$, and $\langle 110 \rangle$. The shape of the $g(\nu)$ for the TA phonons in GaSb [between the TA(L) and TA(X) critical points] was noticeably different from the characteristic shape of

other semiconductors. In order to determine whether this deviation was unique to GaSb or just an artifact of the $g(\nu)$ calculation based on extrapolation from limited neutron data, we have measured the Γ_1 , Γ_{15} , and Γ_{12} components of the second-order Raman spectrum from an oriented GaSb crystal. Several laser wavelengths were used in order to distinguish possible resonance effects which can distort the second-order Raman line shapes.¹³⁻¹⁶

The GaSb sample used was an undoped single crystal. The scattering surface $\langle 1\bar{1}0 \rangle$ was x-ray oriented to $\pm 2^\circ$ and mechanically polished with Syton (Monsanto Chemical Co.) in order to reduce the laser scattering. Both argon and krypton ion lasers were used as the excitation source, and the Raman light was analyzed by a Jarrell-Ash 25-100 double monochromator. A "square pulse" filter (Corion Corporation) was used to reduce further the laser scattering for the 5145-Å measurements. An ITT FW130 photomultiplier was used in conjunction with conventional photon-counting electronics. All measurements were made at room temperature in the backscattering configuration (reflection geometry) with 25° angle of incidence. The sample was mounted in an

TABLE I. Incident-scattered polarization combinations measured in the backscattering configuration from a $\langle 1\bar{1}0 \rangle$ face of GaSb.

Incident polarization	Scattered polarization	Raman components
$\langle 001 \rangle$	$\langle 001 \rangle$	$\Gamma_1 + 4\Gamma_{12}$
$\langle 001 \rangle$	$\langle 110 \rangle$	Γ_{15}
$\langle 111 \rangle$	$\langle 111 \rangle$	$\Gamma_1 + \frac{4}{3}\Gamma_{15}$
$\langle 111 \rangle$	$\langle 11\bar{2} \rangle$	$2\Gamma_{12} + \frac{1}{3}\Gamma_{15}$

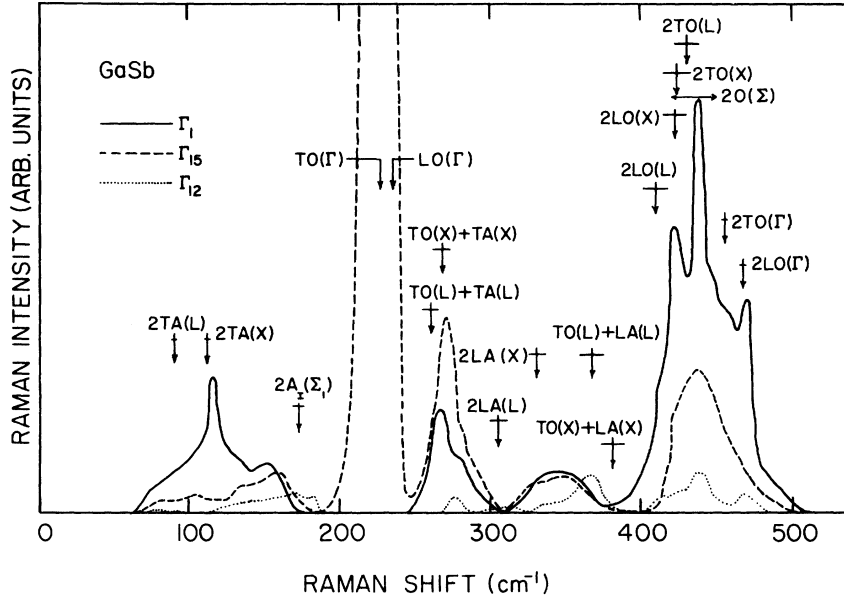


FIG. 1. Second-order Raman spectrum decomposed into the three irreducible components (Γ_1 , Γ_{15} , and Γ_{12}). See Table I for the combinations of incident and scattered polarization used in the decomposition. The arrows specify the frequency (note error bars) of high-symmetry phonon overtones and combinations as determined from the neutron scattering data of Ref. 11. Data taken at 300 °K.

evacuated chamber in order to eliminate interference from the rotational Raman scattering of atmospheric N_2 and O_2 .

Decomposition of the measured spectra into their three irreducible components (Γ_1 , Γ_{15} , and Γ_{12}) required measurements of the Raman data under three of the four combinations of incident-scattered polarization shown in Table I. The fourth polarization combination was used to check con-

sistency. The decomposed spectra taken with 0.5145- μm excitation are shown in Fig. 1. All spectra were corrected for the wavelength response of the instruments and for the Bose-Einstein factor $(1+n)^2$. Since the dispersion of the absorption coefficient is negligible over the entire two-phonon Raman spectrum,¹⁷ no absorption correction was made. The arrows shown in Fig. 1 specify the frequency (note error bars) of high-

TABLE II. Two-phonon Raman selection rules in zinc-blende structures.^a

	$X(\Delta)^b$	$L(\Lambda)$	Σ^c
Overtones			
2TA	$\Gamma_1 + \Gamma_{15} + \Gamma_{12}$	$\Gamma_1 + \Gamma_{15} + \Gamma_{12}$	$\Gamma_1 + \Gamma_{12}$
2LA	$\Gamma_1 + \Gamma_{12}(\Gamma_1 + \Gamma_{12} + \Gamma_{15})$	$\Gamma_1 + \Gamma_{15}$	$\Gamma_1 + \Gamma_{12}$
2TO	$\Gamma_1 + \Gamma_{15} + \Gamma_{12}$	$\Gamma_1 + \Gamma_{15} + \Gamma_{12}$	$\Gamma_1 + \Gamma_{12}$
2LO	$\Gamma_1 + \Gamma_{12}(\Gamma_1 + \Gamma_{12} + \Gamma_{15})$	$\Gamma_1 + \Gamma_{15}$	$\Gamma_1 + \Gamma_{12}$
Combinations			
TA+LA	Γ_{15}	$\Gamma_{12} + \Gamma_{15}$	Γ_{15}
TA+TO	$\Gamma_1 + \Gamma_{15} + \Gamma_{12}$	$\Gamma_1 + \Gamma_{15} + \Gamma_{12}$	$\Gamma_1 + \Gamma_{12}$
TA+LO	Γ_{15}	$\Gamma_{12} + \Gamma_{15}$	Γ_{15}
LA+TO	Γ_{15}	$\Gamma_{12} + \Gamma_{15}$	Γ_{15}
LA+LO	$\Gamma_{15}(\Gamma_1 + \Gamma_{15} + \Gamma_{12})$	$\Gamma_1 + \Gamma_{15}$	$\Gamma_1 + \Gamma_{12}$
TO+LO	Γ_{15}	$\Gamma_{12} + \Gamma_{15}$	Γ_{15}
$A_I(\Sigma_1) + A_{II}(\Sigma_1)$			$\Gamma_1 + \Gamma_{12}$
$O_I(\Sigma_1) + O_{II}(\Sigma_1)$			$\Gamma_1 + \Gamma_{12}$

^a In the case $M_{III} > M_V$, $LO(X)$ and $LA(X)$ change roles.

^b Where selection rules along Δ differ from those at X , those associated with Δ appear in parentheses.

^c Along Σ : LA is replaced by $A_{I,II}(\Sigma_1)$; LO is replaced by $O_{I,II}(\Sigma_1)$; TA and TO are replaced by $TA(\Sigma_2)$ and $TO(\Sigma_2)$, respectively.

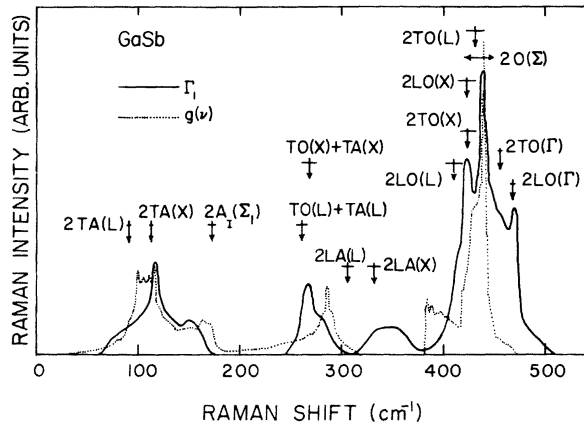


FIG. 2. Comparison of the Γ_1 Raman spectrum (solid lines) with the one-phonon density of states (dotted lines) calculated in Ref. 11.

symmetry phonon overtones and combinations as determined from the neutron measurement¹¹ and from the present Raman data for zone-center modes. The notation is standard; T, L, A, and O indicate transverse, longitudinal acoustic, or optic modes, respectively; I and II indicate mixed modes; and the irreducible representation of each mode is given in parentheses. These spectra for GaSb are similar to those for other diamond and zinc-blende-type semiconductors. The dominant Γ_1 scattering is comprised of four broad features: 2TA (60–170 cm^{-1}); TO+TA (250–310 cm^{-1}); 2LA and LA+LO (310–380 cm^{-1}); and 2LO and 2TO (380–510 cm^{-1}). Table II lists the group-theoretic

selection rules for two-phonon Raman scattering from some high-symmetry points and lines in crystals of zinc-blende structure. For diamond structure crystals, a similar table was tabulated by Temple and Hathaway.²

A comparison of the Γ_1 Raman spectrum with the calculated $g(\nu)$ from Ref. 11 is shown in Fig. 2. It should be noted that the Γ_1 spectrum contains overtones as well as combinations of phonons that have the same symmetry, whereas $g(\nu)$ (with its frequency scale expanded by 2) is the density of phonon states for overtones. However, in the 60–170 cm^{-1} region of the Γ_1 Raman spectrum, mainly overtones of TA contribute and it is therefore reasonable to compare the Raman data with $g(\nu)$. A distinct difference is noted in the region between 2TA(L) and 2TA(X). By examining discrepancies between the SM dispersion curves and the actual neutron data in Ref. 11, reproduced in Fig. 3, one notes that the SM has overestimated the TA($\Lambda \rightarrow L$) frequencies and underestimated the TA(Σ_2) frequencies. These discrepancies resulted in many more modes in the region between 2TA(L) and 2TA(X). Consequently, we believe that the flat top shape in $g(\nu)$ is an artifact of the SM fit and does not make GaSb distinct from other diamond or zinc-blende-type semiconductors which all show a characteristic sharp peak that compares well with the Γ_1 Raman spectrum. Another difference between the Γ_1 Raman spectrum and $g(\nu)$ occurs at the high-energy edge of the 2TA line shape. This edge in the Raman spectrum is shifted to lower energy than the corresponding feature in $g(\nu)$. Again we

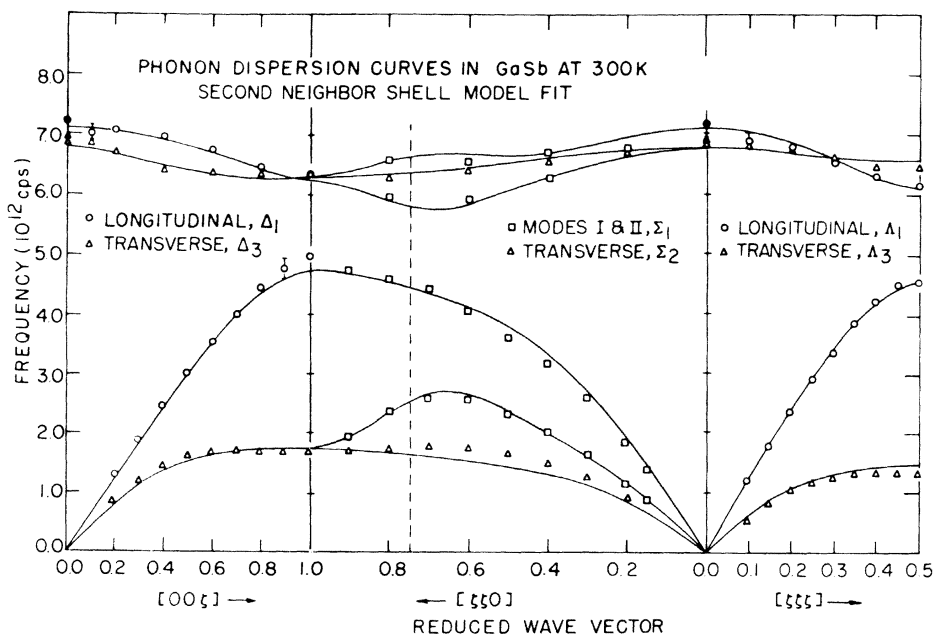


FIG. 3. Neutron scattering measurements (data points) and shell-model fit (solid line) for GaSb from Fig. 2 of Ref. 11.

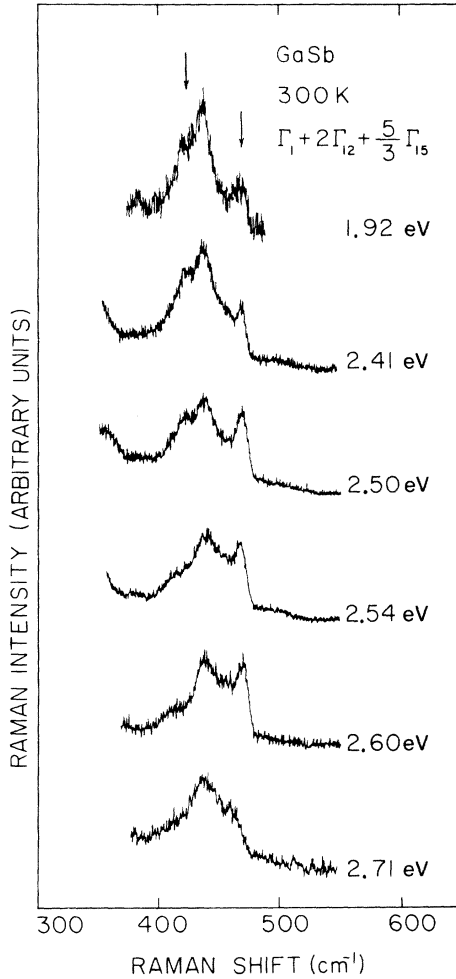


FIG. 4. Evolution of the two-optic phonon Raman line shape with increasing photon energies ($\hbar\omega_i = 1.92$ – 2.71 eV). Note the photon energy dependence of the $2LO(\Gamma)$ (470 cm^{-1}) and the $2TO(\Delta)$ (424 cm^{-1}) peaks marked by the arrows.

believe this difference is due to the overestimation of the SM calculation along $A_1(\Sigma_1)$.

As stated above, the combination of TO + TA (250 – 310 cm^{-1}) and LA + LO (310 – 380 cm^{-1}) can contribute to the Γ_1 Raman spectrum but will not appear in $g(\nu)$. One would need to calculate a two-phonon density of states which includes both combinations and overtones. It is interesting to note that although $g(\nu)$ predicts a zero value for LA(X), the Raman data are relatively strong in the region of $2LA(X)$. The step in the $g(\nu)$ at 380 cm^{-1} and the plateau extending to 400 cm^{-1} , both due to the $O_1(\Sigma_1)$, was not observed, although group-theoretically allowed in the Raman data. The absence of this step is somewhat surprising, considering

that this is the lowest optic frequency critical point. Such a step was observed in the second-order Raman spectrum of GaP.¹ Some of the features of the two-optic Raman spectrum (380 – 510 cm^{-1}) agree reasonably well with those of the $g(\nu)$. In fact, the corresponding peaks at 440 cm^{-1} are well matched.

The two Raman peaks at 424 and 470 cm^{-1} displayed in Figs. 1 and 2 have no corresponding features in $g(\nu)$. The 470 - cm^{-1} peak is attributed to the resonance enhancement of $2LO(\Gamma)$ phonons, due to the close proximity of the 2.41 -eV incident photon energy ($\hbar\omega_i$) to the 2.5 -eV $E_1 + \Delta_1$ gap.¹⁷ The resonance enhancement of $2LO(\Gamma)$ and then the decrease when $\hbar\omega_i$ increases toward and then exceeds the energy of the direct gaps ($E_0, E_0 + \Delta_0, E_1,$ and $E_1 + \Delta_1$) have been reported previously^{6, 7, 13–15} in other semiconductors. The uncorrected spectra in Fig. 4 show the resonant evolution of the 470 - cm^{-1} peak as $\hbar\omega_i$ is increased from 1.92 to 2.71 eV.

Figure 4 also shows the evolution of the 424 - cm^{-1} peak mentioned with regard to Figs. 1 and 2 ($\hbar\omega_i = 2.41$ eV). It is noted that this peak abruptly disappears for $\hbar\omega_i > 2.5$ eV. From the neutron data,¹¹ this 424 - cm^{-1} peak in the Γ_1 spectrum can have contributions from phonons with large wave vector, $2LO(X_1)$, $2TO(X_2)$, $2TO(\Delta_1)$, $2TO(\Sigma_2)$, $O_1(\Sigma_1) + O_{11}(\Sigma_1)$. The lowest conduction band of¹⁸ GaSb along the line Δ has a maximum at 2.5 eV with $\Delta = 0.3X$ and a minimum at 1.5 eV with $\Delta = 0.8X$. The dispersion of the $TO(\Delta)$ phonons for $\Delta \approx 0.3$ – $0.8X$ is reasonably flat, and the frequency of $2TO(\Delta)$ corresponds closely to 424 cm^{-1} . Resonant enhancement of selective pairs of phonons with large wave vector that participate in phonon-assisted transitions has been reported previously in Si,¹⁴ Ge,¹⁵ and AgBr.¹⁹ We postulate at this time that the resonant behavior of the 424 - cm^{-1} peak is a manifestation of a resonance with the indirect gap involving electric dipole transitions from $\Delta_{3v} \rightarrow \Delta_{1c}$ and $\Delta_{4v} \rightarrow \Delta_{1c}$ and phonon-assisted transitions in the valence band from $\Delta_{3v} \rightarrow \Gamma_{15v}$ and $\Delta_{4v} \rightarrow \Gamma_{15v}$. Similar phonon-assisted processes in the conduction band are symmetry forbidden for TO phonons. This above mechanism would explain the disappearance of the 424 - cm^{-1} peak for photon energies above 2.5 eV, as the resonance condition for Δ phonon-assisted transitions can no longer be achieved. Furthermore, the peak would be expected to persist [with only slight frequency shift, due to the flatness of the $TO(\Delta)$ band] down to photon energies comparable to the Δ conduction-band minimum (1.5 eV). We exclude the assignment of this peak as due to the X and Σ phonons mentioned above because there are no apparent features in the electronic band structure associated with

these points that can explain the observed resonance behavior.

In summary, the three irreducible components of the second-order Raman spectrum of GaSb have been measured and compared to the existing one-phonon density-of-states calculation. It was concluded that atypical features of the TA and $O_1(\Sigma_1)$ portion of $g(\nu)$ were artifacts of the shell-model fit of the neutron scattering data. From measurements at several wavelengths, we noted that the line shape of the two-optic Raman spectrum

was altered by resonance effects involving $2LO(\Gamma)$ when $\hbar\omega_i \simeq E_1 + \Delta_1$. Furthermore, it was postulated that the resonance behavior of the $2TO(\Delta)$ peak is a result of resonance with the indirect $\Gamma_{15v} \rightarrow \Delta_{1c}$ gap.

ACKNOWLEDGMENTS

The authors wish to thank Dr. M. K. Farr for his helpful comments on the manuscript. One of us (P.B.K.) is grateful to the NRL-NRC Resident Research Associate program for financial support.

*Supported in part by Office of Naval Research Contract No. N00014-75-C-0866.

- ¹B. A. Weinstein and M. Cardona, *Solid State Commun.* **10**, 961 (1972).
²P. A. Temple and C. E. Hathaway, *Phys. Rev. B* **7**, 3685 (1973).
³B. A. Weinstein and M. Cardona, *Phys. Rev. B* **7**, 2545 (1973).
⁴S. A. Solin and A. K. Ramdas, *Phys. Rev. B* **1**, 1687 (1970).
⁵R. M. Hoff and J. C. Irwin, *Can. J. Phys.* **51**, 63 (1973).
⁶W. Kiefer, W. Richter, and M. Cardona, *Phys. Rev. B* **12**, 2346 (1975).
⁷R. L. Schmidt, B. D. McCombe, and M. Cardona, *Phys. Rev. B* **11**, 746 (1975).
⁸R. M. Hoff and J. C. Irwin, *Phys. Rev. B* **10**, 3464 (1974).
⁹G. Nelin and G. Nilsson, *Phys. Rev. B* **5**, 3151 (1972).
¹⁰G. Nilsson and G. Nelin, *Phys. Rev. B* **6**, 3777 (1972).
¹¹M. K. Farr, J. G. Traylor, and S. K. Sinha, *Phys.*

Rev. B **11**, 1587 (1975).

- ¹²G. Gilet and L. J. Raubenheimer, *Phys. Rev.* **144**, 390 (1966).
¹³B. A. Weinstein and M. Cardona, *Phys. Rev. B* **8**, 2795 (1973).
¹⁴J. B. Renucci, R. N. Tyte, and M. Cardona, *Phys. Rev. B* **11**, 3885 (1975).
¹⁵M. A. Renucci, J. B. Renucci, R. Zeyher, and M. Cardona, *Phys. Rev. B* **10**, 4309 (1974).
¹⁶P. B. Klein, H. Masui, J. J. Song, and R. K. Chang, *Solid State Commun.* **14**, 1163 (1974).
¹⁷M. Cardona and G. Harbeke, *J. Appl. Phys.* **34**, 813 (1963).
¹⁸C. W. Higginbotham, F. H. Pollak, and M. Cardona, in *Proceedings of the Ninth International Conference on the Physics of Semiconductors Moscow 1968*, edited by S. M. Ryvkin (Nauka, Leningrad, 1968), p. 57.
¹⁹W. von der Oster, G. Schaak, and J. Weber, *Solid State Commun.* **15**, 1561 (1974).